UCRL-92635 Rev. 1
PREPRINT

PARAMETRIC STUDY OF WIND GENERATED SUPERMICRON PARTICLE EFFECTS IN LARGE FIRES

William M. Porch
Joyce E. Penner
Lawrence Livermore National Laboratory

Dale A. Gillette
NOAA/ARL

This paper was prepared for submittal to
Atmospheric Environment

February 1985

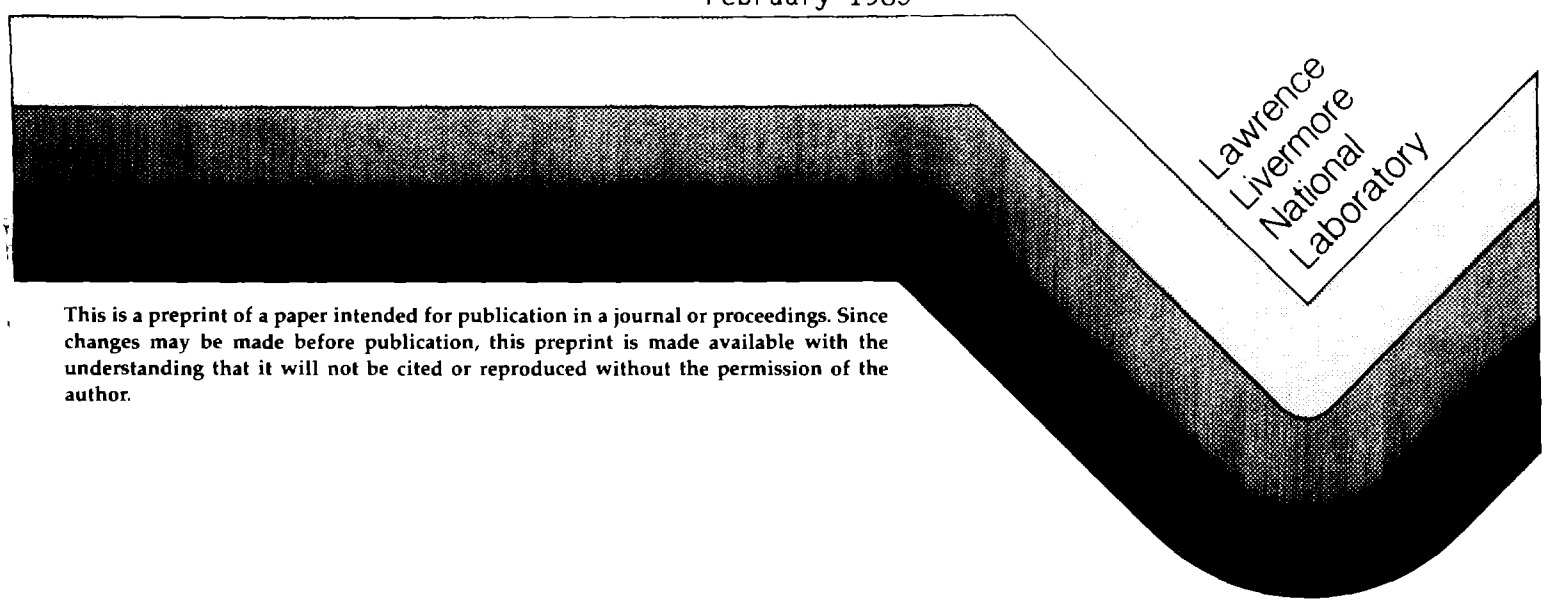

UCRL-92635 rev. 1

PARAMETRIC STUDY OF WIND GENERATED SUPERMICRON PARTICLE EFFECTS IN LARGE FIRES

William M. Porch and Joyce E. Penner
Lawrence Livermore National Laboratory, University of California
Livermore, California 94550

Dale A. Gillette
NOAA/ARL, Boulder, Colorado

February 1985

ABSTRACT

A numerical study is presented of the effects of supermicron particles mechanically generated by large fires on coagulation loss of submicron aerosols in the smoke plumes. This study shows that inclusion of the source generation of large particles in the model can reduce the contribution to the optical depth of submicron particles by a factor of 2 at visible wavelengths. This assumes a combination of high turbulence and high supermicron concentrations. Since no measurements of supermicron concentrations in large firestorms have been made, a concentration corresponding to values found in medium sized dust devils was assumed. This study also shows that the early-time optical effect of the supermicron particles can be considerable in both visible and infrared wavelengths.

INTRODUCTION

In this paper we investigate the importance of a poorly understood component of large fires to the microphysics of aerosol size transformation and the resultant optical effects. This uncertain component is the concentration of mechanically generated aerosols larger than a micron by the winds associated with large fires. The motivation for this work comes from recent attempts to calculate the climatic effect of fires generated by a nuclear exchange (Crutzen and Birks, 1982; Turco et al., 1983). The size distributions assumed in these studies generally simulate aerosol sizes in laboratory-scale fires. Aircraft sampling has recently shown that small-scale controlled burns have a much higher concentration of supermicron particles than that observed in laboratory fires (Radke et al., 1983). Most of these particles are thought to be associated with mechanically generated, partially burned char and larger primary suspendable material at the source. In actual firestorms, the ground surface could also contribute a considerable flux of supermicron particles.

Palmer (1981) reported results of project Flambeau, which simulated wildfire conditions. In that report, he writes of observations of extremely high winds in the fire and strong vorticity. For one 12 hectare fire whirl, Palmer mentioned that the ground was scoured clean, "removing all material smaller than about 1 cm diameter." Palmer concluded that "inside even moderate sized fires, wind may be in excess of 70 m s^{-1} which can loft significant quantities of mineral and fine fuel residues to 1000 m or more."

Wind-blown-dust studies have shown that submicron and supermicron aerosol generation from surfaces is a very strong function of wind speed and turbulence (Gillette, 1974) even during very short wind episodes (Porch and Gillette, 1977). It is, therefore, important to include supermicron particle generation in constructing aerosol concentrations and size distributions that scale to large fires and different surface types.

The microphysical importance of supermicron particles can be considerable. Not only is the proper initial aerosol size distribution important for simulating the early optical effects of fires, but also the large particles serve as coagulation sites for visible-wavelength, optically active particles that are the most long-lived particles in the atmospheric system. Once attached to supermicron particles in the initial concentrated turbulent smoke plume, submicron particles are more easily removed by subsequent precipitation. The cloud-forming, ice-nucleating and/or cloud droplet interaction of the supermicron particles may prove to be the most important microphysical parameter of aerosols from large fires, from a global climate point of view. This is because sedimentation of particles near 10 μm radius raised to midtropospheric heights will take several days for removal if the particles have 1-2 g cm^{-3} density, and much longer if they are fluffy chain aggregates of considerably smaller density.

In this paper, we describe numerical results of time-dependent aerosol size and optical effects from coagulation calculations for a simulated large fire plume with and without a high concentration of supermicron particles. The large-particle generation is based on wind speeds predicted to be associated with firestorms and measured concentrations of wind-blown dust. The coagulation calculations were carried out for the first hour, when high concentrations maximize the effect of the supermicron particles. The calculations include Brownian diffusion, differential settling and turbulent shear mechanisms. Calculations were made with constant concentrations at the source and fixed turbulence levels to compare with simple calculation estimates, as well as time-varying plume dilution and turbulence derived from a hydrodynamic buoyancy-driven transport and diffusion computer code simulating a firestorm (Penner et al., 1985). These calculations were run over a 1 hour time period to compare with simple calculations, however, the first ten to thirty minutes (when the Lagrangian air parcel is within the active fire plume are the most important for scavenging.

The optical effects of the evolving aerosol distribution were calculated at wavelengths of both 0.55 μm and 10 μm. This was done both for the total distribution including submicron and supermicron sizes and for the submicron fraction only, because it is the submicron fraction that is most likely to persist in the atmosphere for time periods long enough to affect global climate. These results do not either validate or invalidate previous estimates of the climatic effect of nuclear fire aerosol, because so little is known of what real supermicron concentrations to expect in a fire storm. But they do focus attention on the need for future calculations and measurements of the importance of supermicron particles and turbulence generated by fire storms.

THEORY AND ASSUMPTIONS

The calculations presented in this paper describe the coupling of a coagulation simulation to a numerical model of fire plume development. Optical depth of the aerosol with changing size distribution is simultaneously calculated. The coagulation calculation uses the slip correction of Fuchs (1964) as formulated by Storebo (1972). Assuming that spherical particles form together with no bounce-off to make an equivalent volume particle, the rate of formation due to Brownian motion is

$$dn_k/dt = 4\pi(r_i + r_j) \cdot (D_i + D_j) \cdot n_i \cdot n_j \cdot \beta_{ij} = K_{i,j} \cdot n_i \cdot n_j \quad (1)$$

for

$$k = i + j$$

where r_i and r_j are the initial particle radii and D_i and D_j are the corresponding diffusion coefficients. β_{ij} is the slip correction term and $K_{i,j}$ is the thermal coagulation coefficient, and n is number of particles.

The diffusion coefficients are derived empirically to include the region where particle slip is important and are functions of absolute temperature, air viscosity and mean free path. β_{ij} is a function of the geometry of interception, the diffusion coefficients and the relative thermal

velocity of the particles. The change in particle density at volume v_j consists of a generation and a loss

$$\frac{dn(v_j)}{dt} = \int_{v_{min}}^{v_j/2} K_{i,j-1} \cdot n(v_i) \cdot n(v_j - v_i) \cdot dv_i$$

$$- n(v_j) \cdot \int_{v_{min}}^{\infty} K_{i,j} \cdot n(v_i) \cdot dv_i \qquad (2)$$

where v_{min} is the smallest particle volume. This formulation was adapted by Blifford et. al (1974) to include sedimentation and shear coagulation through the coagulation coefficient

$$K_{i,j} = K^B_{i,j} + K^T_{i,j} + K^S_{i,j} \qquad (3)$$

where $K^B_{i,j}$ is the Brownian coagulation coefficient used in Equation (1), $K^T_{i,j}$ is the turbulent shear coagulation coefficient, and $K^S_{i,j}$ is the sedimentation differential-settling coagulation coefficient.

$K^T_{i,j}$ and $K^S_{i,j}$ are derived from Friedlander (1965) as

$$K^T_{i,j} = 1.3 \cdot (r_i + r_j)^3 \, (\epsilon/\nu)^{1/2} \qquad (4)$$

where ϵ is the energy dissipation by turbulence and ν is the kinematic viscosity and

$$K^S_{i,j} = (\pi g \rho / 9\mu) \, r_j^2 \, (r_i^2 - r_j^2) \text{ for } r_i \geq r_j \qquad (5)$$

where g is the acceleration due to gravity, μ is the dynamic viscosity and ρ is the effective particle density.

The appropriateness of the turbulent shear coagulation formulation in Equations (4) has been tested at turbulence levels higher than considered

in this paper (Swift and Wells, 1979) This formulation was found to apply to particles in the 0.1 to 10 μm range and was applied to the determination of the removal of submicron aerosol by supermicron particles in a turbulent smoke stack.

Under normal background atmospheric conditions where the concentration of large particles is low and there is little turbulence, $K^{T}_{i,j}$ and $K^{S}_{i,j}$ are negligible compared with thermal coagulation. However, we will show this is not the case in our simulation of a firestorm when high supermicron concentrations and turbulence are assumed.

The numerical code used to calculate the particle size evolution was tested with a self-preserving size distribution (Friedlander, 1965), and a good comparison was found for analytic and calculated particle size evolution in the continuum size ranges. However, until the calculations are tested against the evolution of particles in a fire plume with a high concentration of large particles the appropriateness of even the kinetic coagulation Equation (2) is open to question. Monte Carlo simulations imply that coagulation may be underestimated by Equation (1) for the part of the distribution with small number concentration (i.e., the larger particles) because of the effects of nonuniform spatial distribution of spherical particles (Valioulis and List, 1984). Also, other stochastic aggregation studies (Mountain and Mulholland, 1984) have shown that an underestimation (by a factor of 3 or more) of coagulation may result from using Equation (1). This underestimation is due to the extra-effective area available for collision associated with the branched chain agglomerates almost always found in association with fire-generated aerosols. Also, electrical effects due to the charged aerosols in large fires may be important and are not included in our calculations. Despite these limitations, which imply an even greater supermicron coagulation, a simple calculation supports the potential importance of supermicron particles and turbulent coagulation.

If all the submicron particles could be represented by a single size, and supermicron particles by another size, then Equation (1) could be

applied directly. Also, if the number of the large particles can be assumed to vary only slightly compared with the variation in the number of smaller particles, then the number concentration of small particles as a function of time is simply

$$n(t)_{small} \simeq n_o \, e^{-t(K \cdot n_{large})} \tag{6}$$

where n_o is the initial number concentration of small particles, K is the coagulation coefficient, and n_{large} is the number concentration of supermicron particles.

If the small particle radius is taken as 0.25 μm, Equation (6) is dominated by turbulent shear coagulation in high turbulence with a high supermicron population. With an energy dissipation rate of 8000 $cm^2 \, s^{-3}$ relatively fast reduction of the number of submicron particles is possible. An e-folding time of 20 min corresponds to a concentration of about 5 $g \, m^{-3}$ of 5 μm particles. An energy dissipation rate of 8000 $cm^2 \, s^{-3}$ is about four times the value of ϵ observed in a severe thunderstorm. This upper bound choice seems reasonable, since the vertical shear calculated in a 4 km radius five by cotton (1985) was found to be twice that obtained from modeled thunderstorms. The density of the particles was arbitrarily chosen to be 0.5 $g \, cm^{-3}$ to simulate a mixture of biologically derived fuel residues, aggregates and mineral dust. Alternatively, the same e-folding time would be obtained with only one 200 μm particle in 3 cm^3.

Concentrations of 5 $g \, m^{-3}$ of supermicron particles have been observed in dust devils (Sinclair, 1976). This concentration is representative of Sinclair's "medium sized dust devils" (diameter 9 m and vertical extent 2.3 km). For "large" (23 m diameter and 3 km vertical extent) and "extra-large" (46 m diameter and 3.8 km vertical extent) dust devils, qualitative evidence exists that concentrations of dust are much larger than 5 $g \, m^{-3}$. This concentration is about a factor of 100 times larger than the supermicron concentrations found by Radke et al., (1983). Since the vertical flux of material goes as at least the cube of the wind speed, this

corresponds to an assumption of about a factor of 5 higher winds than those generated by the fires they studied. In this study, we omit water condensation from consideration. However, mass concentrations in the thunderstorms often exceed 5 gm^{-3}. The average concentration in mount Saint Helen's total volcanic cloud power a 6 hour period was estimated to be 9 gm^{-3} from radar studies (Harris and Rose, 1983). We believe the dust devil to be a stronger analog to a rotating firestorm than normal wind erosion. In fact, historical observations indicate "tornadoes of fire" associated with the burning of Williamsonville, WI, in 1871 (Moran and Stieglitz, 1983). Of course, high concentrations of supermicron aerosol assumes the availability of dust from rubblized and falling buildings, ash and partially burned fuel residues within the lareger major fire plume and outside where only partial burning occurs.

In the high winds generaged in the firestorm circulation, much of the entrained material would go directly into suspension (rather than into saltation as observed in dust storms and sand dune movement.) Indeed, wind tunnel data for direct suspension (Gillette, experiment in progress) have been extrapolated to give vertical fluxes of around 0.4 g $cm^{-2}s^{-1}$ for friction velocities of about 205 cm s^{-1} (a not unreasonable value in the extreme conditions of a firestorm). This would give an aerosol loading of a little more than 5 g m^{-3} if a vertical wind of 70 m s^{-1} and a factor of 10 dilution with background air is assumed (based on observations in the Flambeau experiments reported by Palmer (1981) and observations of Bush et al. (1968)). This mass loading number is conservative in the sense that, with higher winds or with less dilution and vertical spreading, the concentration could be much higher. There is, however, only anecdotal evidence to compare dust devil/wind erosion dust with fire storm particle concentrations. It is possible that partially burned biological material from areas already burned is even more erodible than undisturbed soil. These high concentrations of large particles probably only occur in the core of the fire plume, but this is the region where most of the submicron smoke must travel if it is to reach levels of 8-10 km (thereby, avoiding rainout and climate coupling to the earth's surface). Also, the Flambeau experiment

indicated that much of the transport in the fire plume can be associated with organized vorticities like dust devils which are much more efficient in transfering mass from the ground to the atmosphere.

The simple calculation of coagulation loss of submicron aerosols due to high concentrations of supermicron particles is qualitatively similar to the complete size distribution calculations described in the next section. The major limitation of the simple calculation is the inability of a two-particle population model to account for the growth of very small particles into the optically active size range, which serves to somewhat lengthen the depletion time of the optically active particles.

The optical parameters calculated include the optical depth due to absorption and scattering, and the single scattering albedo for wavelengths of 0.55 μm and 10.0 μm. This was done using a computer program developed by Dave (1972), which assumes spherical uniform particles. The indices of refraction for 0.55 μm and 10.0 μm were chosen to be 1.53-0.05i and 4.25-0.4i, respectively, for a forest-fire-type aerosol. Calculations were also made for a visible index of refraction of 1.75-0.3i to simulate urban fire plumes, following Turco et al. (1983). The forest fire refraction indices were chosen based on Patterson and McMahon's (1984) measurements for visible wavelengths from laboratory fires, and the assumption that the ratio of visible to infrared indices for fire aerosol are the same as those measured for soot (Dugin et al., 1981).

Finally, a parametric test was run of the coagulation calculation with and without supermicron aerosol. The physical parameters in the model included an average temperature of 296K, mean free path of 6×10^{-6}, dynamic viscosity of 1.8×10^{-4} and kinematic viscosity of 0.146 (all in cgs units). These values were held fixed in the model because their variability in the fire plume evolution over 1 hour is less important than the other effects tested and because there is much more uncertainty in their estimated values. The submicron size distribution was chosen as log-normal with a geometric mean radius (r_m) of 0.045 μm and geometric standard deviation

(σ_g) of 1.75 on the basis of results of Patterson and McMahon (1984). An initial concentration of 0.05g m^{-3} was assumed for the submicron particles, based on calculations of the smoke density above a large-scale fire storm with intensity 8.9×10^4 W m^{-2} (Penner et al., 1985). This assumes no gas-to-particle conversion in the plume and no supermicron suspension. The individual aerosol density was assumed to be 1 g cm^{-3}, which is close to Patterson and McMahon's (1984) assumed density of 1.3.

The parameters tested include the energy dissipation rate and the size of the wind-generated aerosol (assumed log-normal with a geometric standard deviation of 1.7). Since so little is known about supermicron particles in an active source region of a fire storm, the spread in the distribution is assumed to be the same as that observed in the submicron sizes. At longer times, removal processes will narrow the supermicron distribution spread through elimination of the largest particles. The concentration and density of the supermicron particles were assumed, as in the simple calculation, to be 5 g m^{-3} and 0.5 g cm^{-3}, respectively. The effect of dilution within the plume and evolving turbulence was tested by calculation of these parameters from a hydrodynamic model simulation of the fire plume (Penner and Haselman, 1985).

The hydrodynamic model is available in both a two- and three-dimensional form as described by Haselman (1980). This code has been modified to simulate the plume dynamics above a large-scale fire (Penner et al., 1985). It solves the conservation equations of mass, momentum, energy and species by an explicit method of second-order accuracy. Estimates of average temperature, evolving plume dilution and the changing ratio of energy dissipation by turbulent eddies to kinematic viscosity from this code are then used in the coagulation calculations.

RESULTS

The results of testing the parametric sensitivity of the numerical calculations for the aerosol size evolution in a simulated large-fire plume

are described here. The focus was on the effect of introducing a fixed supermicron mass concentration of 5 g m^{-3} in addition to the submicron distribution. First, we investigate the relative importance of the coagulation mechanisms in Equation (3). Then, we show the effects of the mechanisms on the evolution of the size distribution under varying turbulence and dilution assumptions. Finally, we derive the optical effects of the size evolution at visible and infrared wavelengths.

Table 1 shows a matrix of coagulation coefficients calculated between aerosol particles with given radii. It is obvious that coagulation for submicron particles is dominated by thermal diffusion, but for supermicron particles, under highly turbulent conditions (ϵ=8000 cm^2 s^{-3}), turbulent shear coagulation dominates. The effect of these competitive coagulation mechanisms on the size distribution is shown in Fig. 1. This figure of the evolved size distribution after 1 hour shows an initial double-peaked log-normal distribution with the submicron geometric mean radius r_m at 0.045 μm (0.05 g m^{-3}) and supermicron r_m at 5 μm (5 g m^{-3}). The figure shows that the effect of the turbulent shear coagulation is to reduce the particle concentrations in the intermediate (0.1 to 1 μm) and large sizes, inhibiting the growth rate of very small particles and creating very large particles (over 50 μm). This loss of intermediate-sized particles is a function of the initial size of the supermicron particles assumed and the level of turbulence.

Figure 2 shows the evolution of a hypothetical double-peaked log-normal size distribution with a supermicron particle component having a geometric mean radius (r_m) of 5 μm and mass concentration of 5 g m^{-3}, and a single log-normal distribution with r_m at 0.045 μm and mass concentration of 0.05 g m^{-3}. Two turbulence conditions are plotted with ϵ = 1000 and 8000 cm^2 s^{-3}. The effect of increased turbulence is negligible for the development of a submicron distribution without supermicron particles, but has a sizable effect on the reduction of particles between about 0.2 and 1 μm with supermicron particles. The particles with the highest visible light extinction efficiencies are within this size range. Figure 3 shows

comparable results for the case in which the mass concentration for the supermicron particles peaked at 10 μm instead of 5 μm. The effect of the reduction of the submicron aerosols is still apparent, but reduced. This is because we assumed the same mass concentration in both cases. The aerosol size effect in Equation (4) maximizes the effect for supermicron particles closest in size to the optically active particle radii. Very few size distributions have been measured in large fires, and, as Radke et al. (1983) point out, the largest size particles are notoriously hard to measure because of anisokinetic sampling problems. Size distributions measured close to California brush fires with a piezoelectric cascade impactor sampling device showed large-particle mass-median radii of about 2 to 4.8 μm (Wallace and Chaun, 1976). The larger-particle-size peaks were associated with higher observed winds. The somewhat higher values of r_m used in these calculations were based on laboratory measurements of aerosol sizes most easily suspended from flat surfaces (Punjrath and Heldman, 1972) and are probably different from supermicron particle sizes in a real firestorm.

The calculations shown in Figs. 2 and 3 assume a constant level of turbulence and a constant supermicron particles of plume concentration of 5 g m^{-3}. The e-folding time in the model including dilution was founded to be proportional to the initial supermicron concentration (as found in equation 6). Since the turbulence has a square root dependence, it is not as important as uncertainties in the initial supermicron concentration to scavenging calculations.

The optical effects of these processes are determined from the convolution of the derived distribution functions and the extinction efficiencies. Table 2 shows the evolution of the calculated optical depth due to absorption (τ_a) and scattering (τ_s), referenced to a plume depth of 1 km and single scattering albedo (ω). These parameters are calculated for just the submicron particles and for both the submicron plus the supermicron aerosols. Under the very high assumed concentrations of supermicron particles, these particles contribute significantly to the optical extinction,

especially in the early stages. This is because this size distribution does not fall off faster than $1/r^3$, as is usually the case for supermicron particles in the atmosphere far from sources. Figure 4 shows the evolution of the optical extinction cross section (as a function of size) multiplied by the differential number concentration for the high-turbulence case shown in Fig. 2 without sedimentation, diffusion or precipitation loss of the larger particles. The importance of large-particle optical effect is smaller at visible wavelengths if the supermicron particles peak at larger sizes. It is the submicron fraction of the aerosols that are likely to avoid water cloud/aerosol interaction and sedimentation and therefore are the most likely to exist in the atmosphere long enough to be involved in large-scale climate effects. Table 2 shows that the submicron aerosol mass and optical depth can be significantly reduced by coagulation with larger particles in the first hour of plume development. The major effect of including the supermicron aerosol optical effects in the early stages of plume development is to increase the relative effect of aerosol absorption at visible wavelengths. This may be important in eventual plume height determination if radiative effects are included.

Tables 3 and 4 show the effect of including plume dilution and calculated turbulence levels from the hydrodynamic model of Penner et al. (1985). The effect of dilution alone (Table 3) reduces the relative decrease of submicron optical depths from a factor of about 3 to about 2 for highest turbulence assumption (ϵ = 8000 $cm^2\ s^{-3}$) for initial supermicron concentrations of 5 g m^{-3}. Coupling the calculation with the time varying turbulence and plume dilution estimates derived from the hydrodynamic model simulation of a large-area fire (Penner et al., 1985) showed only small submicron particle reduction (Table 4). This is largely due to much smaller levels of ϵ calculated in the model than the previously assumed values of 1000 and 8000 $cm^2\ s^{-3}$. In the model, values for ϵ begin at about 10 $cm^2\ s^{-3}$ and quickly (within 1.5 minutes) increase to values slightly over 1000 $cm^2\ s^{-3}$; ϵ then varies with time and air parcel trajectories, and has values as high as 2000 and as low as about 10 $cm^2\ s^{-3}$. Since these values are generated from the two-dimensional uniform heating of a large

area, estimates of turbulence are probably low, especially near the fire itself where particle concentrations are the highest. The optical effect for particles with radii less than 1 μm is still considerable, with a reduction of over 10%. However, because of the uncertainty associated with sub-grid scale parameterizations needed to derive ϵ from a large scale model, we believe the effects of dilution and high turbulence shown in Table 3 are more realistic than those shown in Table 4.

The effect of a higher refraction index possibly associated with urban fires is shown in Table 5. This table is analogous to the bottom of Table 2 with an assumed value of ϵ of 8000 $cm^2\ s^{-3}$ and no plume dilution. The assumed index of refraction was 1.75-0.3i as used by Turco et al. (1983) for simulating sooty plumes from urban fire storms. The effect of this higher index of refraction is to increase the total extinction. Also, because the greater index of refraction tends to shift the peak of the submicron optical effects to smaller particles (the supermicron effects are unchanged), the optical effects of shear coagulational losses are proportionately reduced. Figure 5 shows the analogous evolution of the optical effects as a function of size (as shown in Fig. 4) for the higher index of refraction and the relative shift to smaller particle sizes for the submicron part of the distribution.

Table 6 shows results analogous to those in Table 2, but for a wavelength of 10 μm for the optical parameters. Here, the most interesting results are for the supermicron part of the distribution. The optical depths for the total size distribution are almost as high at 10 μm as at 0.55 μm. This implies that, if these particles do persist in the atmosphere, many of the conclusions of atmospheric cooling that ignore infrared effects would have to be revised. Ramaswamy and Kiehl (1985) have shown that the climatic effect of fire aerosol depends strongly on the ratio of aerosol absorption at visible and infrared wavelengths. Of course, if the supermicron particles do persist, then long term optical depths in the visible range would have to be revised, as shown in Table 2.

CONCLUSIONS AND RECOMMENDATIONS

We have found that inclusion of turbulent shear coagulation mechanisms and a high concentration of supermicron particles generated by the winds in highly turbulent fire storms have the following effects on the submicron particles that are likely to persist in the atmosphere long enough to have climatic consequences:

1. A considerable reduction in the number of particles between 0.2 and 1 μm radius in the early plume.

2. An associated decrease in the contribution to the optical absorption and scattering at visible wavelengths for these size particles.

In the early plume, the optical effects of the supermicron particles would greatly exceed those of the smaller particles at visible wavelengths. However, the supermicron particles will be unlikely to persist in the atmosphere unless they consist mostly of very low density chain aggregates. If this were the case, the infrared effect could be comparable with visible extinction.

Earlier studies have neglected supermicron aerosol production as a function of the size of the fire and turbulent shear coagulation. No aerosol size measurements of supermicron particles in firestorms exist. Future measurements will have to be carefully designed to assure isokinetic sampling of the large particles in highly turbulent updrafts. These calculations show that supermicron particle concentrations and turbulent intensities should be part of future calculations and experiments designed to characterize plumes from large fires for climatic impact. The longer term persistence of supermicron particles from fires should also be studied.

ACKNOWLEDGMENTS

This work was performed under the auspices of the U.S. Department of Energy by the Lawrence Livermore National Laboratory under Contract W-7405-Eng-48. The authors would like to thank M. MacCracken, C. Molenkamp, L. Edwards, J. Leone, H. Ellsaesser, P. Connell and R. Turco for their helpful comments on this paper.

Table 1. Matrix of coagulation coefficients ($cm^3\ s^{-1}$ between particle sizes r_1, r_2 (cm) for different coagulation mechanisms and combinations

	r_2					
r_1	1.2×10^{-7}	1.2×10^{-6}	1.2×10^{-5}	1.0×10^{-4}	1.0×10^{-3}	1.0×10^{-2}
Thermal coagulation only						
1.2×10^{-7}	8.9×10^{-10}					
1.2×10^{-6}	1.9×10^{-8}	2.4×10^{-9}				
1.2×10^{-5}	1.0×10^{-6}	1.6×10^{-8}	1.0×10^{-9}			
1.0×10^{-4}	1.5×10^{-5}	1.6×10^{-7}	3.2×10^{-9}	6.4×10^{-10}		
1.0×10^{-3}	1.5×10^{-4}	1.6×10^{-6}	2.8×10^{-8}	2.0×10^{-9}	6.1×10^{-10}	
1.0×10^{-2}	1.5×10^{-3}	1.6×10^{-5}	2.7×10^{-7}	1.7×10^{-8}	1.8×10^{-9}	6.0×10^{-10}
Thermal and turbulent shear coagulation (ϵ = 8000 $cm^2\ s^{-3}$)						
1.2×10^{-7}	8.9×10^{-10}					
1.2×10^{-6}	1.9×10^{-8}	2.4×10^{-9}				
1.2×10^{-5}	1.0×10^{-6}	1.6×10^{-8}	1.0×10^{-9}			
1.0×10^{-4}	1.5×10^{-5}	1.6×10^{-7}	3.6×10^{-9}	3.1×10^{-9}		
1.0×10^{-3}	1.5×10^{-4}	1.9×10^{-6}	3.4×10^{-7}	4.1×10^{-7}	2.4×10^{-6}	
1.0×10^{-2}	1.8×10^{-3}	3.2×10^{-4}	3.1×10^{-4}	3.2×10^{-4}	4.0×10^{-4}	2.4×10^{-3}
Thermal, turbulent shear and sedimentation coagulation (large-particle density 0.5 g cm^{-3} and ϵ = 8000 $cm^2\ s^{-3}$)						
1.2×10^{-7}	8.9×10^{-10}					
1.2×10^{-6}	1.9×10^{-8}	2.4×10^{-9}				
1.2×10^{-5}	1.0×10^{-6}	1.6×10^{-8}	1.0×10^{-9}			
1.0×10^{-4}	1.5×10^{-5}	1.6×10^{-7}	3.6×10^{-9}	3.1×10^{-9}		
1.0×10^{-3}	1.5×10^{-4}	1.9×10^{-6}	3.4×10^{-7}	4.3×10^{-7}	2.4×1^{-6}	
1.0×10^{-2}	1.8×10^{-3}	3.2×10^{-4}	3.1×10^{-4}	3.2×10^{-4}	5.9×10^{-4}	2.4×10^{-3}

Table 2. Optical effects at a wavelength of 0.55 μm and with n = 1.53-0.05i for submicron (submicron plus supermicron) aerosols with a submicron aerosol density of 1 gm cm^{-3}, assuming only dilution at the source and fixed levels of turbulence

	Time (min)	Mass Conc. $\leq 1\ \mu m$ (g cm^{-3})	τ_a	τ_s	ω
ϵ=1000 cm^2 s^{-3}					
No supermicron	0	5.2×10^{-8}	69	196	0.74
aerosols	30	4.9×10^{-8}	80	354	0.82
(0.052 g cm^{-3})	60	4.8×10^{-8}	77	319	0.81
With supermicron aerosols(5 g m^{-3}):					
r_m = 5 μm	0	5.2×10^{-8}	69(782)	196(1040)	0.74(0.57)
	30	1.7×10^{-8}	54(212)	239(426)	0.82(0.67)
	60	1.4×10^{-8}	45(139)	197(308)	0.81(0.69)
r_m = 10μm	0	5.2×10^{-8}	69(418)	196(616)	0.74(0.60)
	30	1.9×10^{-8}	61(122)	272(345)	0.82(0.74)
	60	1.7×10^{-8}	55(91)	235(279)	0.81(0.75)
ϵ=8000 cm^2 s^{-3}					
No supermicron	0	5.2×10^{-8}	69	196	0.74
aerosols	30	4.9×10^{-8}	80	354	0.82
	60	4.8×10^{-8}	76	316	0.81
With supermicron aerosols:					
r_m=5 μm	0	5.2×10^{-8}	69(182)	196(1040)	0.74(0.57)
	30	1.1×10^{-8}	34(119)	150(250)	0.82(0.68)
	60	8.2×10^{-9}	26(74)	117(173)	0.82(0.70)
r_m=10 μm	0	5.2×10^{-8}	69(418)	196(616)	0.74(0.60)
	30	1.3×10^{-8}	43(82)	191(237)	0.82(0.74)
	60	1.1×10^{-8}	36(58)	158(184)	0.82(0.76)

Table 3. Optical effects at a wavelength of 0.55 μm for the same conditions as Table 2, plus plume dilutions calculated from hydrodynamic combustion model for submicron (submicron plus supermicron) aerosols

	Time (min)	Mass Conc. ≤ 1 μm (g cm^{-3})	τ_a	τ_s	ω
ϵ=1000 cm^2 s^{-3}					
No supermicron	0	5.2×10^{-8}	69	196	0.74
Aerosols	30	1.2×10^{-8}	19	80	0.81
(0.052 g cm^{-3})	60	7.7×10^{-9}	14	60	0.81
With supermicron Aerosols(5 g m^{-3}):					
r_m = 5 μm	0	5.2×10^{-8}	69(782)	196(1040)	0.74(0.57)
	30	5.1×10^{-9}	16(115)	67(184)	0.81(0.62)
	60	3.2×10^{-9}	10(58)	45(102)	0.81(0.64)
r_m = 10 μm	0	5.2×10^{-8}	69(418)	196(616)	0.74(0.60)
	30	5.2×10^{-9}	17(52)	69(111)	0.81(0.68)
	60	3.4×10^{-9}	11(27)	48(67)	0.81(0.71)
ϵ=8000 cm^2 s^{-3}					
No supermicron	0	5.2×10^{-8}	69	196	0.74
aerosols	30	1.2×10^{-8}	19	80	0.81
	60	7.7×10^{-9}	13	55	0.81
With supermicron aerosols					
r_m=5 μm	0	5.2×10^{-8}	69(782)	196(1040)	0.74(0.57)
	30	3.8×10^{-9}	12(77)	50(126)	0.80(0.62)
	60	2.2×10^{-9}	7(33)	30(60)	0.81(0.65)
r_m=10 μm	0	5.2×10^{-8}	69(418)	196(616)	0.74(0.60)
	30	4.1×10^{-9}	13(37)	54(83)	0.80(0.69)
	60	2.5×10^{-9}	8(18)	34(47)	0.81(0.72)

Table 4. Optical effects at a wavelength of 0.55 μm with changing dilution and energy dissipation ϵ from a hydrodynamic combustion model for submicron (submicron plus supermicron) aerosols

	Time (min)	Mass Conc. ≤ 1 μm (g cm^{-3})	τ_a	τ_s	w
No supermicron aerosols	0	5.2×10^{-8}	69	196	0.74
	30	1.2×10^{-8}	19	79	0.81
	60	8.3×10^{-9}	14	59	0.81
With supermicron aerosols (5 g m^{-3}):					
r_m = 5 μm	0	5.2×10^{-8}	69(782)	196(1040)	0.74(0.57)
	30	5.5×10^{-9}	18(131)	73(207)	0.81(0.61)
	60	3.8×10^{-9}	12(74)	53(126)	0.81(0.63)
r_m = 10 μm	0	5.2×10^{-8}	69(418)	196(616)	0.74(0.60)
	30	5.7×10^{-9}	18(60)	76(126)	0.81(0.68)
	60	4.0×10^{-9}	13(33)	56(80)	0.81(0.71)

Table 5. Optical effects at a wavelength of 0.55 μm, analogous to Table 2, with the indices of refraction assumed to be n = 1.75-0.3i and ϵ = 8000 cm^2 s^{-3} for submicron (submicron plus supermicron) aerosols.

	Time (min)	τ_a	τ_s	w
No supermicron aerosols:	0	295	230	0.44
	30	212	224	0.51
	60	174	174	0.50
With supermicron Aerosols:				
r_m = 5 μm	0	295(974)	230(1110)	0.44(0.53)
	30	100(181)	109(213)	0.52(0.54)
	60	71(116)	75(133)	0.51(0.53)
r_m = 10 μm	0	295(628)	230(665)	0.44(0.51)
	30	125(161)	135(183)	0.53(0.52)
	60	92(113)	97(124)	0.51(0.52)

Table 6. Optical effects at a wavelength of 10 μm, under the same conditions as in Table 2, with ϵ=8000cm^2 s^{-3} for submicron (submicron plus supermicron) aerosols.

	Time (min)	τ_a	τ_s	w
No supermicron Aerosols	0	2.8	0.32	0.10
	30	3.2	0.69	0.18
	60	3.4	0.83	0.20
With supermicron Aerosols(5 g m^{-3}):				
r_m = 5 μm	0	2.8(709)	0.34(1130)	0.11(0.62)
	30	1.4(83)	0.28(134)	0.17(0.62)
	60	1.1(47)	0.23(75)	0.18(0.61)
r_m = 10 μm	0	2.8(309)	0.32(556)	0.10(0.64)
	30	1.7(35)	0.35(61)	0.17(0.63)
	60	1.5(21)	0.32(35)	0.18(0.63)

References

Blifford I. H., Burgmeier J. W. and Junge C. E. (1974) Modification of aerosol size distributions in the troposphere. Technical Note NCAR-TN/STR98, National Center for Atmospheric Research, Boulder, CO, 64 pp.

Bush A. F., Leonard J. J. and Yundt W. H. (1968) Gas analyses in large fire experiments. Report 68-25, Dept. of Engineering, Univ. Calif. Los Angeles, Los Angeles, CA, 57 pp.

Cotton W. R. (1985) A simulation of cumulonimbus response to a large fire-storm-implication to a nuclear winter. American Scientist, 73, 275-280.

Crutzen P. J. and Birks J. W. (1982) The atmosphere after a nuclear war: Twilight at noon. Ambio 11, 114-125.

Dave J. V. (1972) Development of programs for computing characteristics of ultraviolet radiation technical report--Scaler case. Report FSC-72-0009, NASA, Greenbelt, MD, 37 pp.

Dugin V. P., Toporkov Y. G. and Zadorina N. V. (1981) Laboratory study of the optical properties of soot. Izvestiya, Atmos. Ocean Phys 17, 728-732.

Friedlander S. K. (1965) The similarity theory of the particle size distribution of the atmospheric aerosol. In Aerosol-Physical Chemistry and Applications (edited by K. Spurny), Gordon and Breach, NY.

Fuchs N. A. (1964) The Mechanics of Aerosols. Pergamon Press, Oxford.

Gillette D. A. (1974) On the production of soil wind erosion aerosols having the potential for long range transport. J. Recherches Atmos, 735-744.

Harris, D.M. and W.I. Rose, Jr. (1983) Estimating particle sizes, concentrations, and total mass of ash in volcanic clouds using weather radar. Jn Geophys. Res. 88 (C15), 10,969-10983.

Haselman L. C. (1980) TDC-a computer code for calculating chemically reacting hydrodynamic flows in two dimensions. Report UCRL-52931, Lawrence Livermore National Laboratory, Livermore, CA, 40 pp.

Moran J. M. and Stiedlitz R. D. (1983) Tornadoes of fire: The tragic story of Williamsonville, Wisconsin, October 8, 1871. Weatherwise December, 298-300.

Mountain, R. D. and Mulholland G. W. (1984) Stochastic dynamics simulation Bf particle aggregation. In Proc. of 1st International Symp. on Kinetics of Aggregation and Gelation.

Palmer T. (1981) Large fire winds, gases, and smoke. Atmospheric Environment 15, 2079-2090.

Patterson E. M. and McMahon, C. K. (1984) Absorption characteristics of forest fire particulate matter. Atmospheric Environment (in press).

Penner, J. E. and Haselman L. C. (1985) Smoke inputs to climate models: optical properties and height distribution for nuclear winter studies. Report UCRL-92523, Lawrence Livermore National Laboratory, Livermore, CA. Proceedings of the International Seminar on Nuclear War, August 19-24, 1984, Erice, Italy.

Penner J. E., Haselman L. C. and Edwards L. L. (1985) Buoyant plume calculations. Report UCRL-90915, Lawrence Livermore Laboratory, Livermore, CA, 9 p.

Porch W. M. and Gillette D. A. (1977) A comparison of aerosol and momentum mixing in dust storms using fast-response instruments. J. App. Meteorol. 16, 1273-1281.

Punjrath J. S. and Heldman D. R. (1972) Influence of air turbulence on re-entrainment of small particles from flat surfaces. Trans. A.S.A.E. 559-562.

Radke L., Lyons J., Hegg D., Hobbs P., Sandberg D., and Ward D. (1983) Airborne monitoring and smoke characterization of prescribed fires on forest lands in Western Washington and Oregon. Report EPA 600/X-83-047, EPA, 122 pp.

Ramaswamy V. and Kiehl J. T. (1984) Sensitivities of the radiative forcing due to large loadings of smoke and dust aerosols. Submitted J. Geophys. Res., 49 pp.

Sinclair P. (1976) Vertical transport of desert particulates by dust devils and clear thermals. In Atmosphere-Surface Exchange of Particulate and Gaseous Pollutants (1974) (edited by R. Engelmann and G. Sehmel), ERDA, Oak Ridge, TN, 497-527.

Storeby P. B. (1972) Steady state aerosols. Geofysiska Publikasjoner Geophysica Norvegica (Oslo) 28, p. 101.

Swift, D.L. and Wells, W.H. (1979) Coagulation rates of submicron particulates in the troposphere. Dept. of Environ. Health Sci., Johns Hopkins Univ., Baltimore, MD. NTIS PB-295 756.

Turco R. P., Toon O. B., Ackerman T. P., Pollack J. B. and Sagan C. (1983) Nuclear winter: Global consequences of multiple nuclear explosions. Science 222, 1283-1292.

Valioulis I. A. and List E. J. (1984) A numerical evaluation of the stochastic completeness of the kinetic coagulation equation. J. Atmos. Sci., 41, 2516-2529.

Wallace, D. and R. Chaun (1976) A cascade impaction instrument using quartz crystal microbalance sensing elements for "real time" particle size distribution studies. Presented 8th Materials Research Symposioum, September 24-25.

Captions

Figure 1. The number distribution of an initial, assumed double-peaked log-normal size distribution. The small particle peak is at r_m = 0.045 μm, σ_g = 1.75 and the large particle peak at r_m = 5 μm, σ_g = 1.7; the initial mass concentrations are 0.05 and 5 g m^{-3}, respectively, after 60 min. The plots show the relative effect of Brownian thermal, turbulent shear and differential sedimentation coagulation mechanisms.

Figure 2. The initial distribution described in Fig. 1 and subsequent (after 60 min) concentrations for a distribution without the supermicron peak compared with the distribution in Fig. 1 with all three coagulation mechanisms and two levels of turbulent energy dissipation rates (8000 and 1000 cm^2 s^{-3}).

Figure 3. An initial distribution with the same small-particle peak and a supermicron-particle peak with r_m = 10 μm, σ_g = 1.7 for the same mass concentration as in Fig. 1. The plots show the distribution after 60 min with all turbulent mechanisms and ϵ = 8000 cm^2 s^{-3} compared with that of the initial distribution with no supermicron peak.

Figure 4. Differential optical cross section and size number distribution (C_{ext} as a function of size multiplied by the differential number concentration) evolution in time for a double-peaked initial aerosol size distribution and the same coagulation mechanisms used in Fig. 2, but with ϵ 8000 cm^2 s^{-3} and n = 1.53-0.05i.

Figure 5. Same as Fig. 4, but for n = 1.75-0.3i.

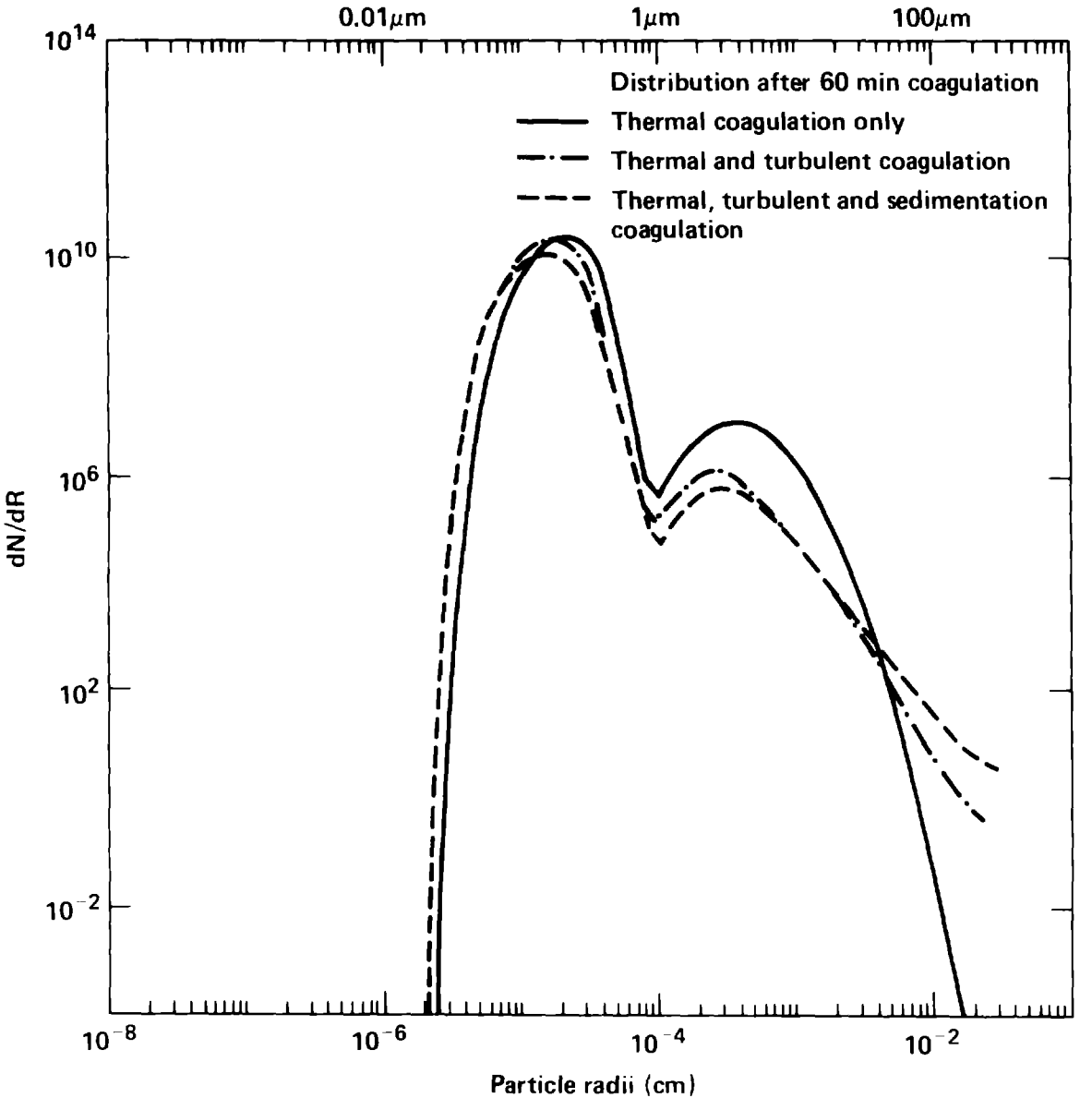
0.01μm
1μm
100μm
10^{14}
10^{10}
10^{6}
10^{2}
10^{-2}
dN/dR
Distribution after 60 min coagulation
Thermal coagulation only
Thermal and turbulent coagulation
Thermal, turbulent and sedimentation coagulation
10^{-8}
10^{-6}
10^{-4}
10^{-2}
Particle radii (cm)

Figure 1

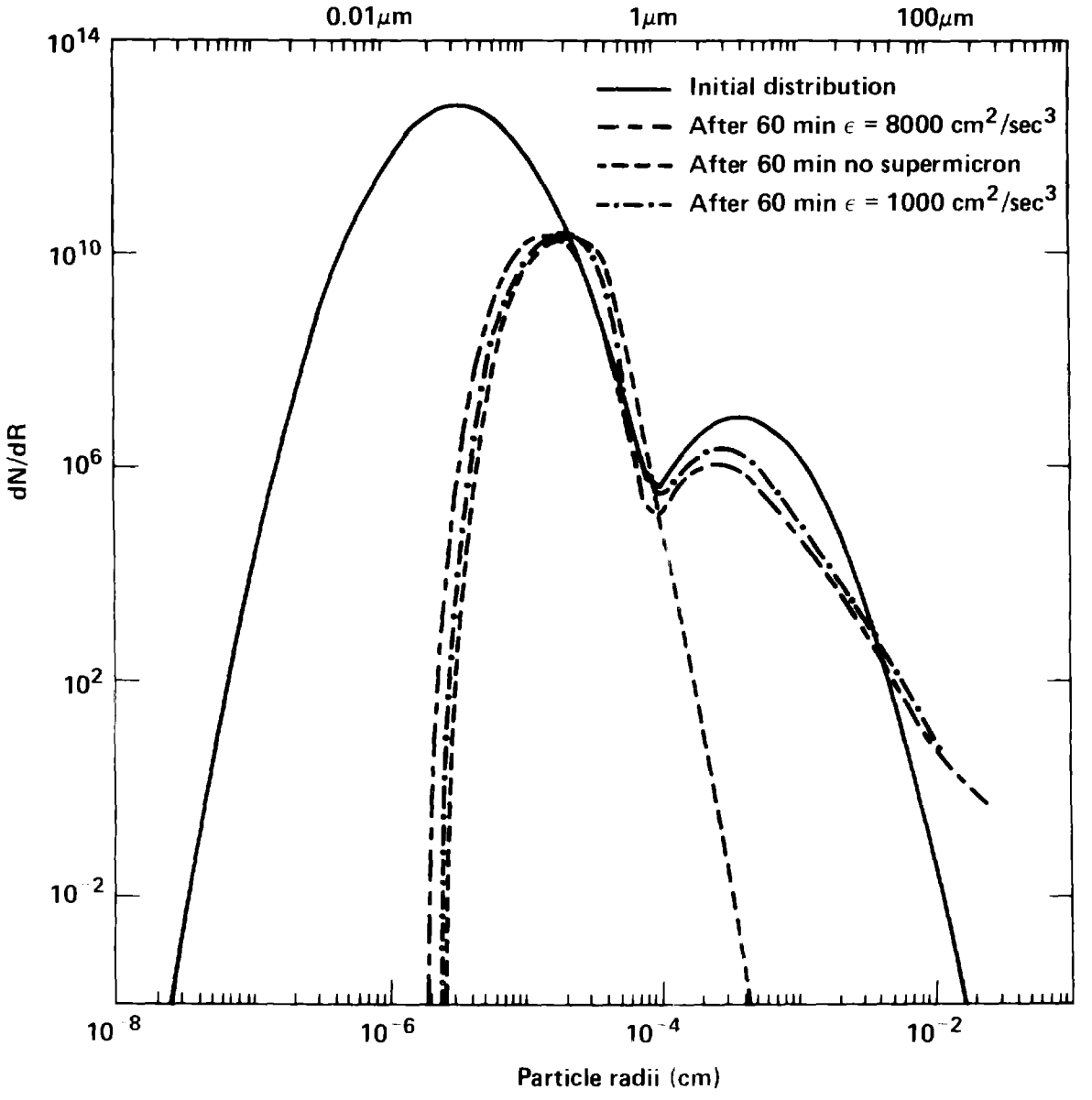
0.01μm
1μm
100μm
Initial distribution
After 60 min ϵ = 8000 cm²/sec³
After 60 min no supermicron
After 60 min ϵ = 1000 cm²/sec³
dN/dR
Particle radii (cm)

Figure 2

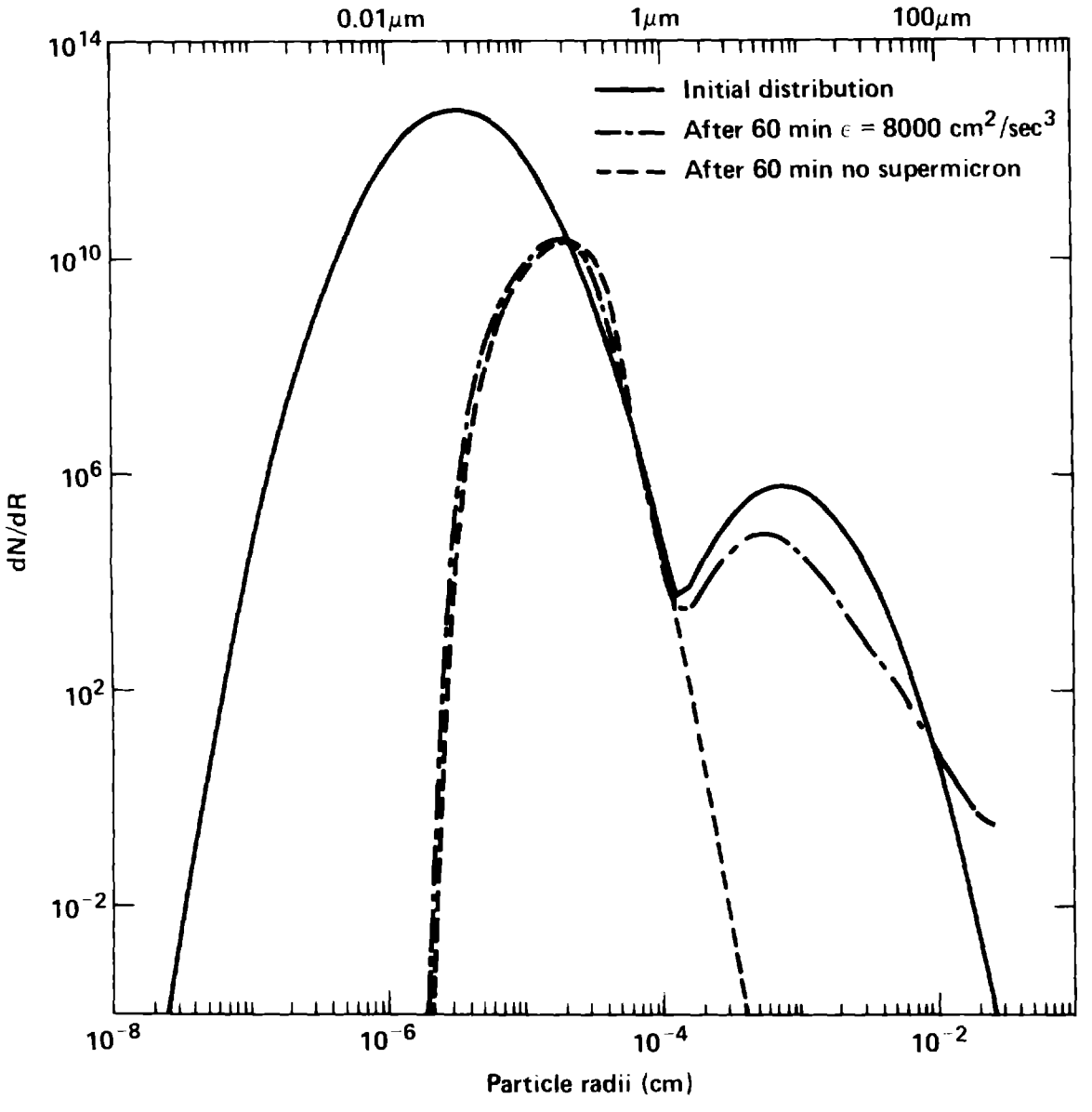
0.01μm
1μm
100μm
10^{14}
10^{10}
10^{6}
10^{2}
10^{-2}
dN/dR
Initial distribution
After 60 min ϵ = 8000 cm²/sec³
After 60 min no supermicron
10^{-8}
10^{-6}
10^{-4}
10^{-2}
Particle radii (cm)

Figure 3

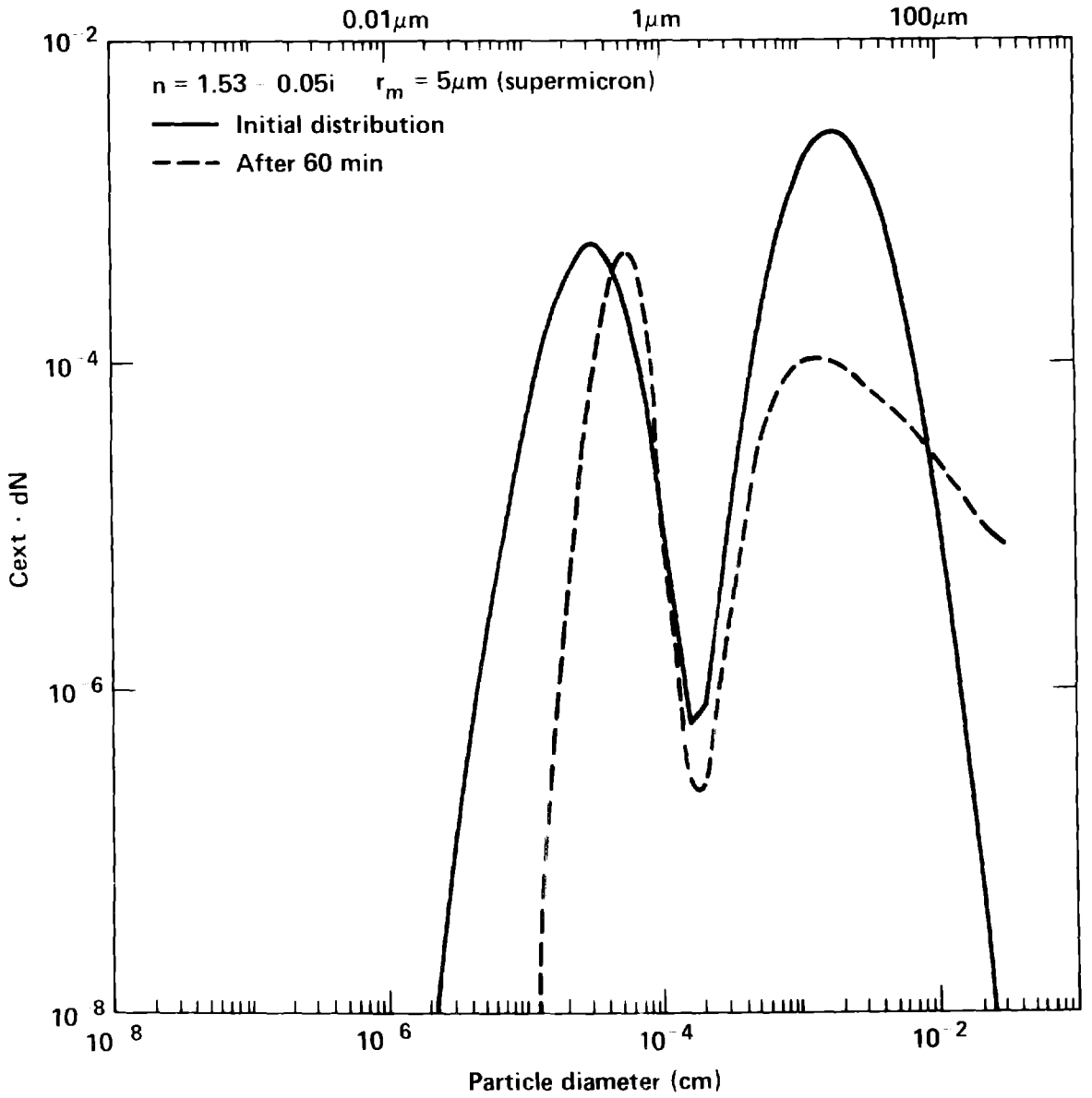
0.01μm
1μm
100μm
10^{-2}
n = 1.53 - 0.05i r_m = 5μm (supermicron)
Initial distribution
After 60 min
10^{-4}
10^{6}
10^{8}
Cext · dN
10^{8}
10^{6}
10^{-4}
10^{-2}
Particle diameter (cm)

Figure 4

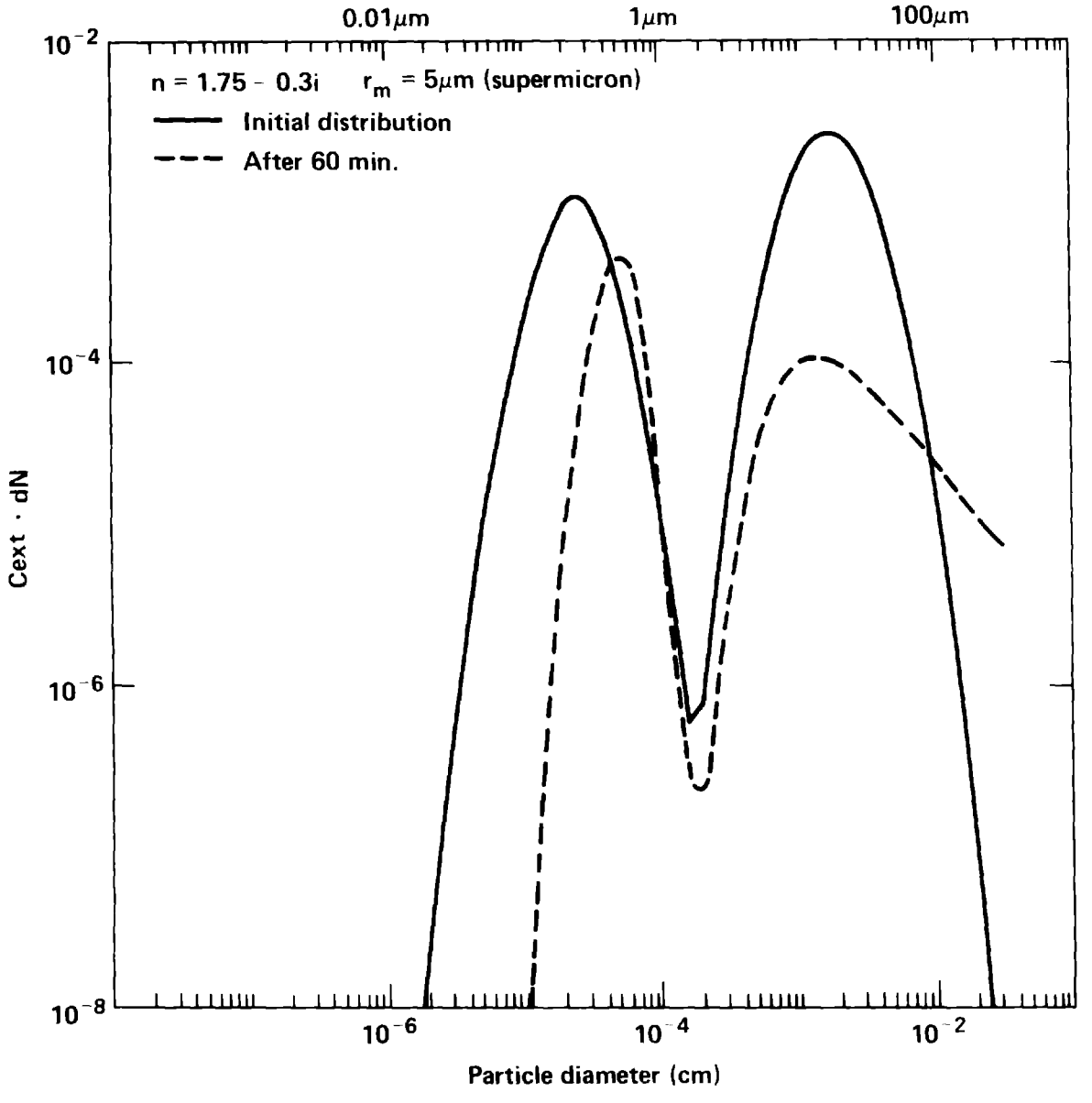
0.01μm
1μm
100μm
10^{-2}
n = 1.75 - 0.3i r_m = 5μm (supermicron)
Initial distribution
After 60 min.
10^{-4}
10^{-6}
10^{-8}
Cext · dN
10^{-6}
10^{-4}
10^{-2}
Particle diameter (cm)

Figure 5